

Vol. 3 • No. 11 • November • 2013

www.advenergymat.de

ADVANCED ENERGY MATERIALS

WILEY-VCH

Light Trapping in Ultrathin Monocrystalline Silicon Solar Cells

Ki Jun Yu, Li Gao, Jae Suk Park, Yu Ri Lee, Christopher J. Corcoran, Ralph G. Nuzzo, Debashis Chanda,* and John A. Rogers*

Ultra-thin monocrystalline silicon solar cells are attractive due to their potential to achieve high efficiency operation and efficient materials utilization, in forms that are mechanically flexible and lightweight. We present the design and fabrication of cells of this type, in which bulk wafers serve as sources of material for ~3 μm thick bars of silicon that include patterns of surface relief, antireflection coatings and back reflectors collectively configured to maximize absorption via trapping of light. Even with unoptimized patterns of doping and designs for electrical contacts, these devices yield power conversion efficiencies of ~8.5%, corresponding to a ~190% enhancement over those of otherwise identical cells without light trapping schemes. Integrating such cells into large-scale arrays on sheets of plastic yield lightweight, mechanically flexible modules, with properties that could facilitate transport and installation and/or enable use in portable applications.

Silicon (Si) remains the material of choice for photovoltaic (PV) applications due to a favorable set of electrical and optical properties, excellent lifetime/reliability, low costs in

manufacturing and high natural abundance.^[1,2] Performance in commercially available cells already approaches the theoretical limit.^[3–5] As a result, research on silicon photovoltaics often now focuses on cost effective means for manufacture, schemes for efficient materials utilization, and unusual methods for integration of silicon into modules.^[6–11] Routes to ultrathin silicon in designs optimized for light management, i.e. light trapping and antireflection, are valuable in this context. Such types of ultra-thin cells are additionally attractive because they offer other attributes such as mechanical flexibility and rugged construction, when mounted on plastic substrates.^[12,13] Notable advances in recent years include methods for kerf-less production of thin wafers from silicon boules by controlled fracture,^[14–17] and for fabrication of ultrathin bars and sheets of silicon from wafers by anisotropic etching.^[8–11,18,19] The most advanced demonstrations of the second strategy involve thin (~6 μm), microscale cells (μ -cells) that incorporate light trapping structures (LTSs) and anti-reflection coatings (ARCs).^[20] The present work introduces refined fabrication techniques that enable further reductions of thickness by more than a factor of two, and light trapping (LT) schemes that exploit engineered cavity resonances between a top surface LTS and a bottom back-side reflector (BSR). By comparison to previous results, these devices offer not only more than a doubling of the efficiency in materials utilization, but also an order of magnitude reduction in bending stiffness.^[21] The latter enables use in ultra-compliant, flexible modules and a reduction in the minimum bend radius by a factor of two. We note that it is difficult to quantitatively compare efficiency results presented here with those from previously reported microcells that have related, but somewhat different, designs.

The fabrication starts with a P-type Czochralski Si <111> wafer (1–10 $\Omega\text{-cm}$, 450 μm thickness, Virginia Semiconductor). The first step involves lithographically patterning arrays (180 \times 14, over an area of 1 cm^2) of microbars (0.59 mm length \times 0.25 μm width) aligned perpendicular to the Si <110> direction. Inductively coupled plasma reactive ion etching (ICP-RIE) in the regions between the bars (strips with 80 μm widths) yields trenches with depths of ~3.3 μm . For each bar, solid state doping of boron (Boron, BN-1250, Saint Gobain) along lengths of $L_{p+} = 60 \mu\text{m}$ and phosphorus (Phosphorus, PH-1000N, Saint Gobain) along lengths of $L_{n+} = 0.5 \text{ mm}$, at 1000 $^{\circ}\text{C}$ (25 min) and 950 $^{\circ}\text{C}$ (10 min), respectively, through patterned hard masks of SiO_2 (900 nm), produces rectifying P-N junctions. Conformal deposition of bilayers of SiO_2 (100 nm)/ SiN_x (500 nm) by plasma-enhanced chemical vapour deposition (PECVD, PlasmaTherm SLR) followed by annealing at 400 $^{\circ}\text{C}$ for 30 min establishes etch barriers on the top surfaces of the bars, as well

K. J. Yu, J. S. Park, Y. R. Lee
Department of Electrical and Computer Engineering
Frederick Seitz Materials Research Laboratory
University of Illinois at Urbana-Champaign
Urbana, IL 61801, USA

L. Gao
Department of Material Science and Engineering
Frederick Seitz Materials Research Laboratory
University of Illinois at Urbana-Champaign
Urbana, IL 61801, USA

C. J. Corcoran, Prof. R. G. Nuzzo
Department of Chemistry
Frederick Seitz Materials Research Laboratory
University of Illinois at Urbana-Champaign
Urbana, IL 61801, USA

Prof. D. Chanda
NanoScience Technology Center
College of Optics and Photonics (CREOL)
University of Central Florida
Orlando, FL 32816, USA
E-mail: debashis.chanda@creol.ucf.edu

Prof. J. A. Rogers
Department of Materials Science and Engineering
Electrical and Computer Engineering
Chemistry, Bioengineering, and Mechanical Science and Engineering
Beckman Institute for Advanced Science and Technology
Frederick Seitz Materials Research Laboratory
University of Illinois
Urbana, Illinois 61801, USA
E-mail: jrogers@illinois.edu



DOI: 10.1002/aenm.201300542

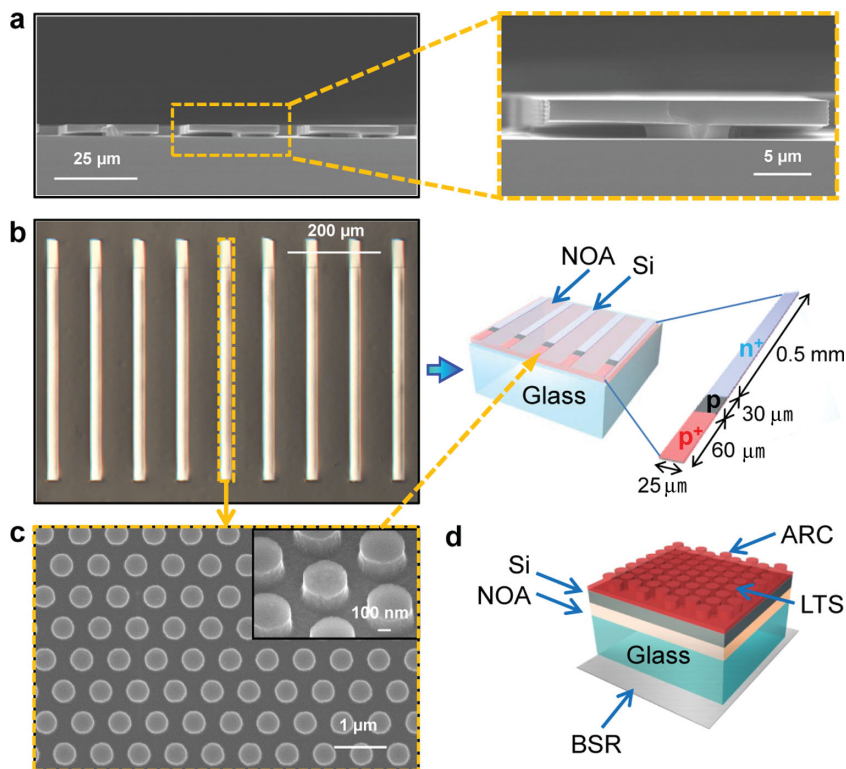


Figure 1. (a) Side view SEM image of ultrathin μ -cells ($\sim 3 \mu\text{m}$). Arrays of μ -cells after partial undercut etching from the surface of a bulk wafer (left). Magnified views of a single μ -cell (right). (b) Optical image and schematic diagram of arrays of μ -cells. The pink and blue areas correspond to regions of p-type and n-type doping. (c) SEM image of top surface light-trapping structures (LTSs). (d) Full light trapping (LT) μ -cell structure, including ARC, LTS, and BSR.

as the sidewalls and bottoms of the etched trenches. Directional deposition of Cr (100 \AA)/Au (1000 \AA) by electron beam evaporation (Tumesal, FC 1800) at an angle of $\pm 30^\circ$ coats the sidewalls and top surfaces, to allow selective removal of the exposed $\text{SiO}_2/\text{SiN}_x$ in the trenches by reactive-ion etching (CHF_3 (40 sccm)/ O_2 (2 sccm); 50 mtorr, 150 W, 15 min). Immersing the processed wafer into a solution of potassium hydroxide (PSE-200, Transene) etches the silicon preferentially along the $\langle 110 \rangle$ direction, starting at the exposed bottoms of the trenches, thereby producing arrays of freely suspended microbars tethered to the underlying wafer at their ends. Boron doping (1000°C for 5 min) using the residual layers of $\text{SiO}_2/\text{SiN}_x$ as a mask yields a back surface field, thereby completing the fabrication of collections of functional solar μ -cells. This overall process has yields of $\sim 99\%$. A scanning electron microscope (SEM; Hitachi s4800) cross sectional image of a wafer after partial undercut etching of an array of μ -cells appears on the left in **Figure 1(a)**, with a magnified view of an individual μ -cell on the right. **Figure 1(b)** presents an optical image of an array of μ -cells (left) and a schematic illustration (right). Each μ -cell is $25 \mu\text{m}$ wide, 0.59 mm long, and $\sim 3 \mu\text{m}$ thick. The pink, grey, and blue areas in this illustration correspond to boron doped ($I_{p+} = 60 \mu\text{m}$), un-doped ($I_p = 30 \mu\text{m}$), and phosphorus doped ($I_{p+} = 0.5 \text{ mm}$) regions respectively. After transfer printing onto a substrate of interest, soft imprint lithography and etching define LTSs on the top surfaces of the μ -cells. **Figure 1(c)** provides top-view SEM images

of LTSs consisting of a hexagonal lattice of cylindrical posts of silicon, with periodicity, diameter and height of 500 nm , 370 nm and 120 nm , respectively. A bilayer of SiN_x (35 nm) and SiO_2 (50 nm) deposited by PECVD serves as an ARC. Furthermore, A layer of silver ($\sim 200 \text{ nm}$) deposited on the backside of the glass substrate provides a BSR. (Previous work^[20] involving μ -cells with $6 \mu\text{m}$ thicknesses did not incorporate the cavity layout that is enabled by this BSR.) Additional options for the BSR range from other metals to diffuse white reflectors. **Figure 1(d)** illustrates schematically the layers that constitute a completed μ -cell. The NOA (NOA 74, Norland Products Inc) in this figure is a thin, transparent layer of a photo-curable polyurethane that bonds the cells to the glass substrate (1 mm thick).

Three dimensional finite difference time domain (FDTD) techniques and optical absorption measurements quantitatively reveal the roles of the LTS, the ARC and the BSR. The FDTD simulations assume a $3 \mu\text{m}$ thick film of silicon with infinite lateral extent. The top hexagonal pattern diffracts/scatters light to increase the optical interaction length and, by consequence, the absorption. The BSR further increases this length and also establishes cavity resonances. Some of the higher order diffracted/scattered light remains trapped inside the silicon via total internal reflection at the top surface. In both FDTD and experiment, the absorption (A) corresponds to $A = 1 - T - R$ where T and R are the transmission and reflection, respectively. **Figure 2(a)-(b)** compares the relative absorption (with respect to the solar AM1.5D spectrum) for $3 \mu\text{m}$ thick μ -cells with and without the light trapping scheme (i.e. bare vs LT), evaluated using FDTD and experimental measurements with an AM 1.5D solar spectrum. The absorption measurements are limited to wavelengths between 550 nm and 1100 nm by the source-detector combination in our microscope-coupled FTIR system (Bruker Vertex 70-Huperion 1000). The simulated and measured absorption values, integrated over the spectrum, are 27.6% (**Figure 2(a)**) and 28% (**Figure 2(b)**), respectively, for the bare μ -cell; with the LT μ -cell, these values increase to 69% and 77% respectively. The graph in **Figure 2(c)** shows in an absolute scale that much of the absorption enhancement due to light trapping appears near the band edge, as expected, where bare silicon is weakly absorbing. The thin geometry of the μ -cells leads to Fabry-Perot cavity resonances^[22] in both bare and LT cases. The LT configuration, however, greatly enhances these effects. Here, the combined presence of the top diffractive pattern associated with the LTS and the bottom BSR induces not only resonances associated with 0^{th} order diffraction but with the 1^{st} diffracted order as well. Moreover, these and other higher diffraction orders remain trapped due to total internal reflection. The FDTD simulation assumes perfect arrays of nano-posts as

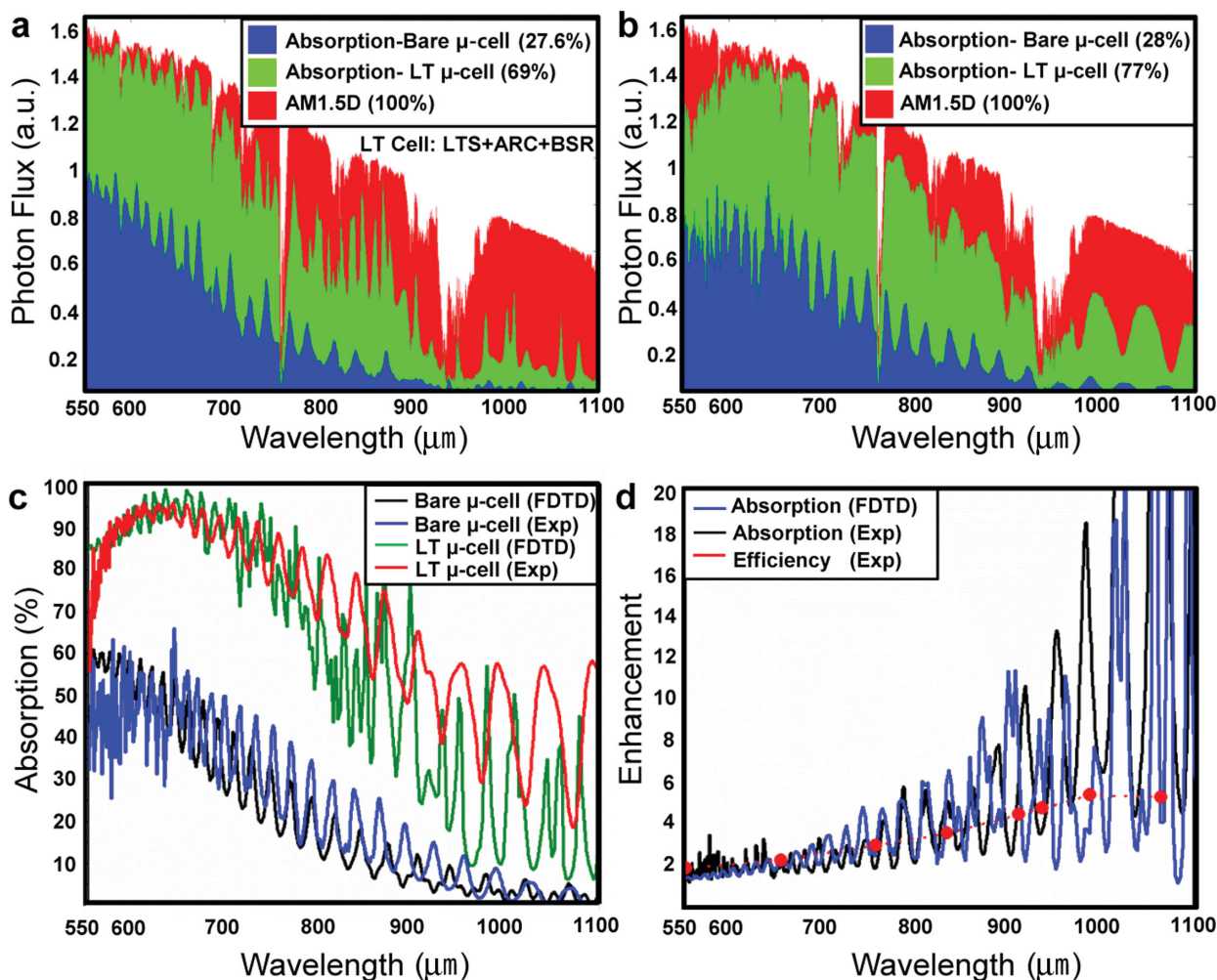


Figure 2. (a) Experimentally measured and (b) simulated absorbed photon flux for illumination by the AM 1.5D reference spectrum as a function of wavelength for bare Si, and bare Si with ARC+LTS+BSR. (c) Comparison of absolute absorption of a bare μ-cell and a LT μ-cell as a function of wavelength. (d) Spectrally resolved enhancement in measured and simulated absorption and measured energy conversion efficiency for a LT μ-cell and a bare μ-cell.

the diffractive top surfaces of the microcells. These structures diffract the incident solar spectrum as multiple diffraction orders inside the silicon. In actual cells, the nano-posts possess non-ideal surface profiles due to imperfections associated with the lithography and dry etching processes. These imperfections scatter light in excess of that expected by diffraction alone, thereby leading to additional absorption. The slight discrepancies between experimental observations and FDTD predictions are likely due to such non-idealities of the etched surface relief geometries, thickness variation across the wafer and finite lateral geometries of the μ-cells.

To further understand the spectral aspects of light trapping, we examined the wavelength dependence of enhancements (compared to the bare case) in both absorption and efficiency. Figure 2(d) presents experimental and FDTD results. Simulated and measured enhancements in absorption exhibit sharp narrow band Fabry-Perot cavity resonances. Wavelength dependent efficiency measurements, however, involve illumination over a range of wavelengths (bandwidth ~100 nm) centered at 550 nm, 650 nm, 750 nm, 850 nm, 950 nm, 1050 nm.

Here, spectral averaging eliminates resonances in the efficiency enhancement spectrum. The averaged responses and the overall trends exhibit good agreement between absorption and efficiency enhancement.

Figure 3(a) shows the measured current density (J) as a function of voltage (V) for various μ-cell designs, using simulated AM 1.5D illumination of 1000 W/m^2 at room temperature. For accurate measurements, a lithographically defined pattern of metal (Cr/Au: ~10 nm/200 nm) about the same size of the cell serves as an aperture to prevent exposure of the cells to unwanted, parasitic light. The active area is equal to the cell area. Separate studies isolate the effects of the LTS, ARC and BSR, and their combinations. The samples include: bare Si, with ARC, with BSR, with BSR+ARC, with LTS, with LTS+ARC, with LTS+BSR and, finally, with LTS+BSR+ARC (i.e. LT μ-cell). The data in Figure 3(a) yield key properties that can be considered individually. First, and most simply, is the short circuit current (J_{sc}). This quantity can be expressed as^[23]

$$J_{sc} = qg_{op} (L_p + L_n) \quad (1)$$

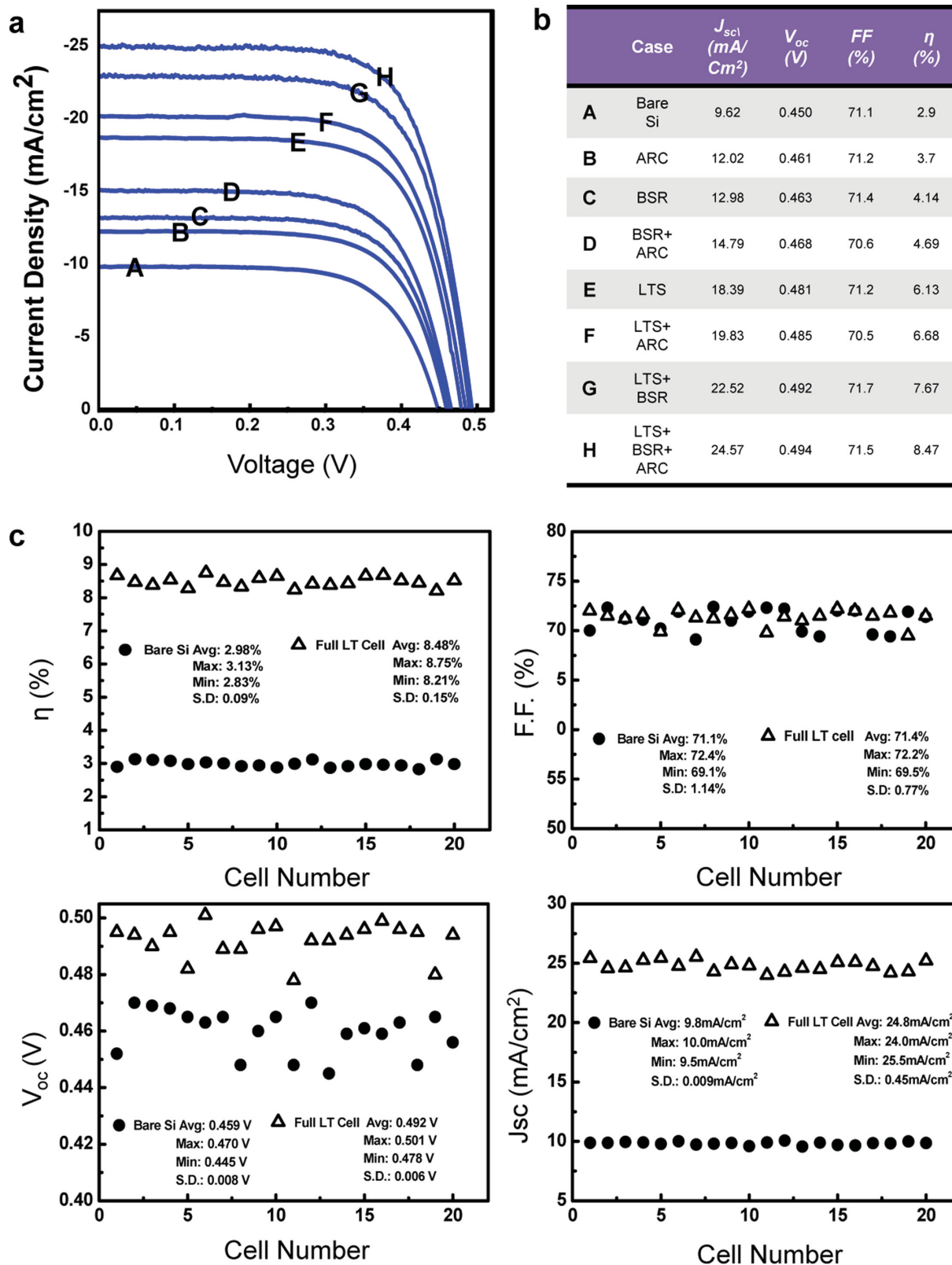


Figure 3. Experimentally measured (a) Current density (J)-Voltage (V) curves for μ -cells with bare Si, and with ARC, BSR, BSR+ARC, LTS, LTS+ARC, LTS+BSR, and LTS+BSR+ARC. (b) Chart of short circuit current (J_{sc}), open circuit voltage (V_{oc}), and efficiency (η) in μ -cells with bare Si, and with ARC, BSR, BSR+ARC, LTS+BSR, and LTS+BSR+ARC. Also shown in the efficiency enhancement with full LT compared to the case of bare Si. (c) Statistical variations in η , FF, V_{oc} , and J_{sc} extracted from measurements on 20 bare μ -cells and 20 full LT μ -cells.

where q is the charge of an electron/hole, g_{op} is the optical generation rate, and L_p and L_n are the minority carrier diffusion lengths. The minority carrier diffusion lengths are determined largely by the materials quality, the doping profiles and the surface properties. Among the devices corresponding to the data of Figure 3(a), all such parameters are roughly the same. As a result, trends in J_{sc} should follow those in g_{op} , or, equivalently, the absorption. As shown in the table of Figure 3(b), J_{sc} of bare Si and bare Si with LTS+BSR+ARC are 9.62 mA/cm² and 24.57 mA/cm², respectively. The enhancement of J_{sc} of bare Si compared to that of the LT cell (LTS+BSR+ARC) is ~155%, which is consistent with both FDTD predicted and experimentally measured enhancements in absorption, i.e. $((69\%)/(27.6\%) \times 100 - 100)\% = 150\%$) and $((77\%)/(28\%) \times 100 - 100)\% = 175\%$), respectively, according to the data of Figure 2 (a),(b).

The open circuit voltage (V_{oc}) is another important parameter. Under assumptions similar to those for Equation (1), this quantity can be written:^[24]

$$V_{oc} = \frac{nkT}{q} \ln \left(\frac{L_p + L_n}{L_p p_n / \tau_p + L_n n_p / \tau_n} g_{op} + 1 \right) \quad (2)$$

where n is the ideality factor, k is the Boltzmann constant, T is the temperature, p_n and n_p are the minority carrier concentrations, τ_p and τ_n are the minority carrier life time, and q , L_p , L_n , and g_{op} are the same parameters as stated in J_{sc} equation. As for the case of J_{sc} the examined μ -cells differ mainly in g_{op} . The expectation, then, is that V_{oc} should vary according to $\ln(cg_{op}+1)$ where c is a constant. The V_{oc} of μ -cells built with bare Si and with LTS+BSR+ARC are 0.45 V, and 0.494 V respectively, as in the table of Figure 3(b). The increase corresponds to ~10%, roughly consistent with the expected weak, logarithmic scaling. The fill factors (FF) for all cases are between 70.5% and 71.5%, with no systematic variations. FF is the ratio of maximum power (P_{max}) to the product of V_{oc} and J_{sc} . The results suggest, then, that P_{max} increases by an amount approximately equal to that of the product of V_{oc} and J_{sc} , consistent with dominant effects of changes in the optical generation rate (g_{op}) associated with different cell configurations as shown in Figure 3(a). Finally, the corresponding measured energy conversion efficiencies are 2.90, 3.7, 4.14, 4.69, 6.13, 6.68, 7.67 and 8.47% for various cases, as tabulated in Figure 3(b). The LTS+BSR+ARC configuration yields the highest overall energy conversion efficiency, consistent with combined effects of enhancements in J_{sc} (~155%) and V_{oc} (~9.78%). The result is that the efficiency of this full LT μ -cell is ~190% larger than that of the bare case. These results are well outside of statistical distributions of results from multiple μ -cells. As an example of the typical variations, Figure 3(c) shows efficiencies (η), fill factor (FF), open circuit voltage (V_{oc}), and short circuit current (J_{sc}) measured in 20 bare μ -cells and 20 μ -cells with the LTS, ARC, and BSR. The efficiencies are ~3.0% +/-0.1% and 8.5% +/-0.2% for the bare μ -cell and the full LT μ -cell case, respectively. Average values of FF for both cases are ~71%, with standard deviations of ~1%. The V_{oc} values are 0.46 V +/-0.01 V and 0.49 V +/-0.01 V for the bare and full LT cases; the J_{sc} values are 9.8 mA/cm² +/-0.01 mA/cm² and 24.8 mA/cm² +/-0.04 mA/cm², respectively.

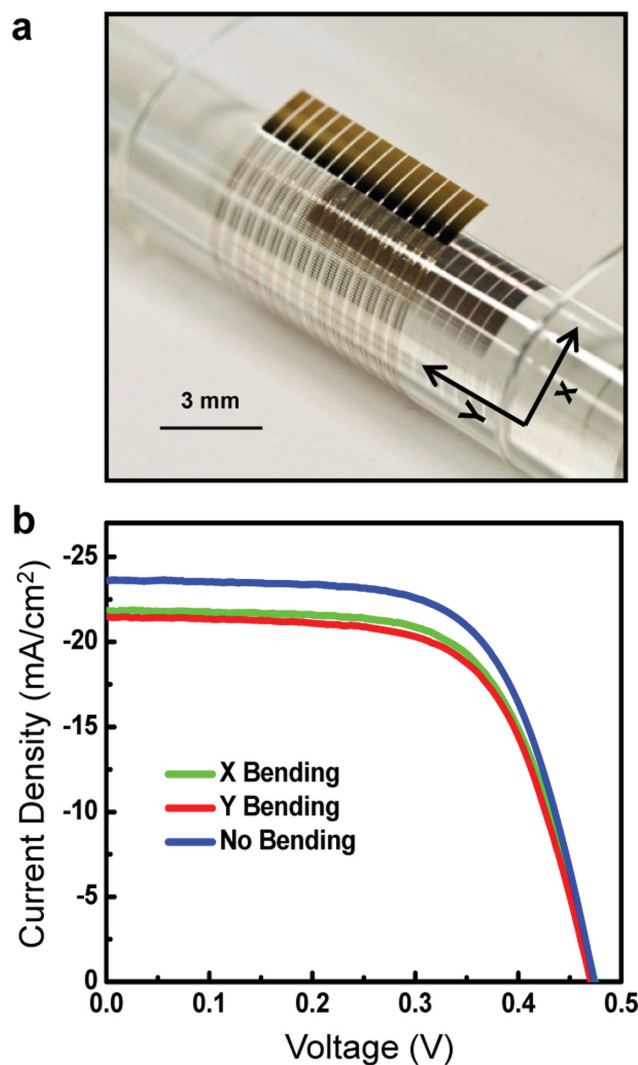


Figure 4. (a) Photograph of a solar mini-module consisting of 108×14 ultrathin μ -cells on a transparent substrate of polyethylene terephthalate (PET, 30 μm) wrapped onto a cylindrical support. (b) Current density (J)-Voltage (V) curves for the flat state and for bending along the x-axis and y-axis to a bend radius of 2.5 mm, for a device with 20 full LT μ -cells connected in parallel.

In addition to efficient materials utilization, ultrathin μ -cells enabled by LT designs and fabrication processes reported here offer other attractive attributes such as mechanical bendability when mounted on plastic substrates. The small thickness is advantageous in this context because (i) the flexural rigidity, which is proportional to the cube of the thickness, is small,^[25,26] (ii) the peak strains associated with bending, which are proportional to the thickness, are small for a given bend radius,^[27] and (iii) the ability to heterogeneously integrate silicon on plastic, for example, improves due to energy release rates for interface failure that reduce linearly with thickness.^[28,29] **Figure 4(a)** shows arrays of such thin cells printed on a thin polymeric substrate bent around a curved surface with a radius of curvature of ~2.5 mm. **Figure 4(b)** represents the J - V characteristics of miniature modules contain 20 μ -cells

with the full LT schemes connected in parallel, in a flat state, bent along the x-direction and, bent along the y-direction relative to the direction of the electrical interconnects. Changes in the illumination condition with bending lead to slight changes in the J_{sc} , but without any irreversible alteration in system performance. The excellent bendability in these systems confirms the value of thin geometries; they also suggest that the nanoposts structures do not have significant detrimental effects on the mechanical robustness. Bendability at this level, particularly when combined with good photovoltaic performance, efficient materials utilization and lightweight construction, could be important for many applications in portable power.

The methods reported here demonstrate the ability to construct monocrystalline silicon solar cells with exceptionally low thicknesses, and in bendable formats. The cavity enhanced LT designs enable absorption of ~77% of A. M. 1.5D illumination, even at thicknesses of ~3 microns. By point of comparison, recently reported arrays of Si microwires^[30] with the same volumetric content of silicon as a 2.8 μm thick planar sheet, achieve somewhat higher levels of absorption (~85%) although at the expense of requirements for less well established routes to forming working cells with good performance characteristics. Collectively, the results suggest further opportunities in research on these and other unusual schemes^[31,32] for implementing silicon in photovoltaic devices, and on related ideas in flexible inorganic photovoltaics.^[32–34]

Acknowledgements

This work was supported by the Energy Frontier Research Center program of the Office of Science of the Department of Energy under Grant DESC0001293. K. J. Yu would like to thank A. J. Baca, R. H. Kim, J. C. Shin, J.-W. Jeong, and B. H. Kim for valuable comments and help. This article was modified after online publication to correct the spelling of author Christopher J. Corcoran's name.

Received: May 16, 2013
Published online: July 3, 2013

- [1] D. M. Bagnall, M. Boreland, *Energy Policy* **2008**, *36*, 4390.
- [2] M. A. Green, *Third Generation Photovoltaics: Advanced Solar Energy Conversion*, Springer **2005**.
- [3] R. M. Swanson, *Conference Record of the 31st IEEE PVSC* **2005**.
- [4] W. Shockley, H. J. Queisser, *J. Appl. Phys.* **1961**, *32*, 510.
- [5] C. H. Henry, *J. Appl. Phys.* **1980**, *51*, 4494.
- [6] A. Shah, P. Torres, R. Tscharnner, N. Wyrsh, H. Keppner, *Science* **1999**, *285*, 692.
- [7] L. V. Mercaldo, M. L. Addonizio, M. Della Noce, P. D. Veneri, A. Scognamiglio, C. Privato, *Appl. Energy* **2009**, *86*, 1836.
- [8] A. J. Baca, K. J. Yu, J. Xiao, S. Wang, J. Yoon, J. H. Ryu, D. Stevenson, R. G. Nuzzo, A. A. Rockett, Y. Huang, J. A. Rogers, *Energy Environ. Sci.* **2010**, *3*, 208.
- [9] J. Yoon, A. J. Baca, S. I. Park, P. Elvikis, J. B. Geddes, L. F. Li, R. H. Kim, J. L. Xiao, S. D. Wang, T. H. Kim, M. J. Motala, B. Y. Ahn, E. B. Duoss, J. A. Lewis, R. G. Nuzzo, P. M. Ferreira, Y. G. Huang, A. Rockett, J. A. Rogers, *Nat. Mater.* **2008**, *7*, 907.
- [10] H. C. Ko, A. J. Baca, J. A. Rogers, *Nano Lett.* **2006**, *6*, 2318.
- [11] A. J. Baca, M. A. Meitl, H. C. Ko, S. Mack, H. S. Kim, J. Y. Dong, P. M. Ferreira, J. A. Rogers, *Adv. Funct. Mater.* **2007**, *17*, 3051.
- [12] M. Pagliaro, R. Ciriminna, G. Palmisano *Chem Sus Chem* **2008**, *1*, 880.
- [13] A. W. Blakers, T. Armour, *Sol. Energy Mater. Sol. Cells* **2009**, *93*, 1440.
- [14] S. W. Bedell, D. Shahrjerdi, B. Hekmatshoartabari, K. Fogel, P. Lauro, N. Sosa, D. Sadana, *IEEE J. Photovoltaic* **2011**, *37th IEEE* **2011**, 228.
- [15] F. Dross, A. Milhe, J. Robbelein, I. Gordon, P. Bouchard, G. Beaucarne, J. Poortmans, *Proceedings of the 2008 IEEE Photovoltaics Specialist Conference* **2008**.
- [16] F. Henley, S. Kang, Z. Liu, L. Tian, J. Wang, Y. L. Chow, in: *34th IEEE Photovoltaic Specialists Conference* **2009**, 1718.
- [17] R. A. Rao, L. Mathew, S. Saha, S. Smith, D. Sarkar, R. Garcia, R. Stout, A. Gurmu, E. Onyegam, D. Ahn, D. Xu, D. Jawaraini, J. Fossum, S. Banerjee, *Proceedings of the 2011 IEEE Photovoltaics Specialist Conference* **2011**.
- [18] K. J. Weber, A. W. Blakers, (Aranda, Australia), Australian National University, ACT, Australia, 10432936 PCT/AU01/01546, Nov **2001**, Appl. #11/193,183, 29 July **2005**.
- [19] P. J. Verlinden, A. W. Blakers, K. J. Weber, J. Babaei, V. Everett, M. J. Kerr, M. F. Stuckings, D. Gordeev, M. J. Stocks, *Sol. Energy Mater. Sol. Cells* **2006**, *90*, 3422.
- [20] D. Shir, J. Yoon, D. Chanda, J. H. Ryu, J. A. Rogers, *Nano Lett.* **2010**, *10*, 3041.
- [21] S. I. Park, J. H. Ahn, X. Feng, S. Wang, Y. Huang, J. A. Rogers, *Adv. Funct. Mater.* **2008**, *18*, 2673.
- [22] O. S. Heavens, *Optical properties of thin solid films*, Dover Publications **1991**.
- [23] <http://www.pveducation.org> (accessed December 2012).
- [24] G. Streetman, S. Banerjee, *Solid State Electronic Devices*, 6th ed, Prentice hall: Upper Saddle River, NJ, **2000**.
- [25] L. D. Landau, E. M. Lifshitz, *Theory of Elasticity*, Vol. 7 (3rd ed.). *Butterworth-Heinemann*, **1986**, pp. 42.
- [26] K. R. Symon, *Mechanics*, 3rd ed, Addison-Wesley, **1971**.
- [27] D. Y. Khang, H. Jiang, Y. Huang, J. A. Rogers, *Science* **2006**, *311*, 208.
- [28] A. M. Kiefer, D. M. Paskiewicz, A. M. Clausen, W. R. Buchwald, R. A. Soref, M. G. Lagally, *ACS Nano* **2011**, *5*, 1179.
- [29] J. H. Ahn, H. S. Kim, K. J. Lee, S. Jeon, S. J. Kang, Y. G. Sun, R. G. Nuzzo, J. A. Rogers, *Science* **2006**, *314*, 1754.
- [30] M. D. Kelzenberg, S. W. Boettcher, J. A. Petykiewicz, D. B. Turner-Evans, M. C. Putnam, E. L. Warren, J. M. Spurgeon, R. M. Briggs, N. S. Lewis, H. A. Atwater, *Nat. Mater.* **2010**, *9*, 239.
- [31] R. J. Knuesel, H. O. Jacobs, *Proc. Natl. Acad. Sci.* **2010**, *107*, 993.
- [32] C. M. Hsu, C. Battaglia, C. Pahud, Z. Ruan, F. J. Haug, S. Fan, C. Ballif, Y. Cui, *Adv. Energy Mater.* **2012**, *2*, 628.
- [33] Z. Fan, H. Razavi, J. Do, A. Moriwaki, O. Ergen, Y.-L. Chueh, P. W. Leu, J. C. Ho, T. Takahashi, L. A. Reichertz, S. Neale, K. Yu, M. Wu, J. W. Ager, A. Javey, *Nat. Mater.* **2009**, *8*, 648.
- [34] K. Nakayama, K. Tanabe, H. A. Atwater, *Appl. Phys. Lett.* **2008**, *93*, 121904.